Investigation of the electronic structure of the Sigma 5(210) grain boundary in silicon by the linear muffin-tin orbitals/tight-binding method

1992 J. Phys.: Condens. Matter 4 2775

(http://iopscience.iop.org/0953-8984/4/11/007)

J. Phys.: Condens. Matter 4 (1992) 2775–2791. Printed in the UK

Investigation of the electronic structure of the Σ5 {2 1 0} grain boundary in silicon by the linear muffin-tin orbitals/tight-binding method

A V Nikolaeva†, A V Artemyev‡, Yu H Vekilov§, L K Fionova‖ and M B Samsonova§

† Institute of Nuclear Safety, Russia Academy of Sciences, 52 Bolshaya Tulskaya, 113191 Moscow, Russia.

‡ Institute of Crystallography, Russia Academy of Sciences, 59 Leninsky Prospekt, 117333 Moscow, Russia.

§ Moscow Steel and Alloys Institute, 4 Leninsky Prospekt, 117936 Moscow, Russia.

‖ Institute of Problems of Microelectronics Technology and Superpure Materials, Russia Academy of Sciences, 142432 Chernogolovka, Moscow Region, Russia.

Received 15 May 1991, in final form 25 October 1991

Abstract. The electronic structure of the Σ5 {2 1 0} grain boundary in silicon was calculated by the first-principles, self-consistent, linear muffin-tin orbitals/tight-binding representation method on the basis of the atomic structure simulated by the bond orbital model. The calculated electronic structure is found to have localized and resonant defect states, which are caused by the distortions of the atomic structure at the grain boundary. Sharply localized states in the pseudo-gap were observed along with splitting of s states and dissipation of s–p mixed states. A rehybridization effect was revealed at the grain boundary on the atoms with strongly distorted bonds. However, there are no states inside the band gap. The increase of the s-state occupancy in comparison with the p-state occupancy appeared on the atoms with strongly distorted bonds at the grain boundary. The relationship between local electronic structure and local arrangement of the atoms is discussed.

1. Introduction

Recently there has been increasing interest in the investigation of the atomic and electronic grain-boundary structure in semiconductors. Most such investigations have been executed with the use of the semi-empirical tight-binding methods. For example, the recursion method was used for the calculation of the electronic structure of the Σ3 {2 1 1} and Σ5 {3 1 0} grain boundaries in silicon [1, 2] and the Σ3 {2 1 1} boundary in germanium [3]. A number of grain boundaries in silicon were investigated with the use of the extended Hückel method in the cluster approach [4, 5]. The Chadi semi-empirical tight-binding method [6, 7] in the framework of the supercell technique was applied for the Σ3 {2 1 1} [8], Σ5 {3 1 0} [9] and Σ9 {2 1 1} [10] boundaries in silicon.

It is very convenient to use such methods for the treatment of a system with a complex and large unit cell, owing to the simplicity of the computational procedure. However, they have certain deficiencies; in particular, the free parameters of the method are fitted by suitable properties of a perfect crystal. In the case of a distorted lattice, a considerable change in the electron density is possible in the crystal and such an approach becomes

0953-8984/92/112775 + 17 $04.50

rather approximate. Moreover, it is obvious that the semi-empirical method can be used for the structure defect calculation of experimentally well studied crystals only. Therefore, a more general and correct investigation of the electronic structure of crystal defects is provided by the *ab initio* methods of solid-state theory.

In these schemes the only input parameters are the atomic number and crystal structure, in contrast with the semi-empirical approach. However, the use of the conventional *ab initio* methods, such as the Korringa–Kohn–Rostoker (KKR) method [11] and augmented plane-wave (APW) one [12], for the investigation of complicated defect structures is limited to a small size of supercell because of the extremely large computer resources needed. The modern, generalized linear muffin-tin orbital (LMTO) Green function method for the calculation of the interface electronic structure was proposed in [13–15]. Unfortunately, the application of this technique is limited by the consideration of the join between two phases with an ideal structure at the interface. The effects connected with the relaxation of the atomic structure at the interphase boundary are omitted. Thus, obviously, it is impossible to use it for grain boundaries, where the real atomic structure of the interface is important.

An attempt to use the first-principles method based on the density-functional theory (DFT) within the local-density approximation (LDA) in the framework of the local orbital basis and the norm-conserving pseudopotential [16] was made in [17] for the $\Sigma 9\ \{2\,2\,1\}$ grain boundary in silicon. However, this method provides for an inadequate description of the fundamental gap of an ideal crystal, causing a significant underestimation of both the direct and band-gap width [16, 17]. This disadvantage is critical in the case of the investigation of the electronic structure of grain boundaries, where the behaviour of the electronic states in this region is most important. Moreover, this method estimates the bond energy in an ideal crystal of silicon with an error of 10–17% (depending on the type of orbital basis set) [16], which can cause a significant error in the determination of the grain-boundary energy.

One of the most perspicacious methods for the calculations of the electronic structure of defects is the LMTO method in the tight-binding representation (LMTO TB method) developed by Andersen [18, 19]. This method provides for: (i) a high speed of calculations that allows one to carry out a first-principles investigation of complicated objects; (ii) a high precision in the determination of the parameters of the band structure (accuracy of about 1% of the bandwidth) and cohesive energy; and (iii) a minimal thickness of the supercells of an artificial crystal for the imposition of periodicity in the direction normal to the boundary plane. This is possible because of the strong localization of LMTO TB basis functions.

In this paper we present the first application of an efficient self-consistent *ab initio* technique based on the LMTO TB method using a supercell geometry for the calculation of the electronic structure at relaxed interfaces on the example of the $\Sigma 5\ \{2\,1\,0\}$ grain boundary in silicon. We have chosen this boundary as an object for our investigations for the following reasons. Firstly, there is no reliable information on its electronic structure. Secondly, this boundary together with the $\Sigma 5\ \{3\,1\,0\}$ boundary, investigated in [2, 9], determines basal structure units in the class of symmetric $\langle 1\,0\,0\rangle$ boundaries [20]. So, its electronic structure may be characteristic of the essential features of boundaries of this class.

2. Method

2.1. The atomic structure simulation

The determination of the equilibrium atomic geometry at a grain boundary requires a value of the total energy calculation such that methods with a high computational

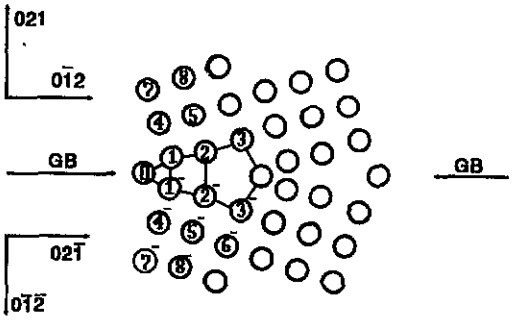

Figure 1. Relaxed atomic structure of the Σ5 {2 1 0} boundary. Full lines denote bonds between atoms in the structure elements of the grain boundary. The projection of the plane of the grain junction is marked by the arrows with the symbols GB. Numbers of the atoms are given in the circles.

complexity cannot be used. So we use a simple bond orbital model for the computer simulation of the atomic structure [21–23]. This model possesses an ability for high speed of computations and provides for a realistic description of the grain-boundary structure in silicon [24]. The computer simulation of the Σ5 {2 1 0} atomic structure included two stages. In the first stage the rigid-body translation was determined, i.e. the mutual position of the grains corresponding to the minimum energy was obtained. The relative coordinates of the individual atoms were not changed. The component of the rigid-body translation in the direction normal to the boundary was equal to 0.02 nm with an accuracy of 0.005 nm. In the direction of the tilt axes ⟨1 0 0⟩ it was equal to 0.042 ± 0.005 nm. It is necessary to note that the shift in the boundary plane disturbs the initial symmetry of the boundary plane.

After a rigid-body translation, an atomic relaxation was carried out by a static procedure with the use of the method of conjugated gradients [25]. The thickness of the operational volume, in which the changes of individual atomic coordinates were calculated, in the direction normal to the boundary plane was equal to 4 nm. We have used the conjunction with the {2 1 0} planes of an ideal crystal, which can be shifted by an interaction with the operational volume, as the boundary condition in this direction. In the boundary plane, periodic boundary conditions [25] were used. We have considered the same periodicity for the grain-boundary structure as that for the {2 1 0} planes in a single crystal. So, we did not take into account the possibility of reconstruction of grain-boundary structure with increase in the periodicity. The relaxation was completed when the maximum value of the gradients of the atomic energy became less than 0.1 eV nm^{-1}.

The simulated atomic structure is shown in figure 1. It is characterized by the absence of dangling bonds, the maximum bond tension of 3.9% between atom 2 and atom 2^{-}, and the maximum deviation of the angle between the interatomic bonds at atom 0 (of 19.5°) from the single-crystal value.

2.2. The method of electronic structure calculation

The first-principles calculation of the electronic structure of a solid can be divided into two parts, i.e. the solution of the Schrödinger equation with a definite crystalline potential to determine the energy band structure and eigenfunctions, and the construction of the crystalline potential. The development of the crystalline potential for a many-electron system is a rather complicated task, and only the density-functional formalism based on the Hohenberg and Kohn theorem [26] in practice gives an acceptable method of self-consistent solution of this problem. It is a formidable computational task and for objects with a complex atomic structure the problem of optimization of the algorithm for its solution becomes very urgent. In particular, the choice of the most suitable type of basis wavefunctions is the way to optimize the computational algorithm.

The basis functions of the LMTO TB method provide for the most effective solution of this problem because of their linearity (independence on energy) and short range, which is essential for the calculation of the electron structure of defects by the supercell technique. These extremely compact basis functions were obtained by an exact transformation of the conventional LMTO basis functions [19]. They decrease exponentially with relative interatomic distance instead of as the inverse power in the case of the LMTO basis functions. The size of the supercells, modelling the structure of crystals with defects, can be decreased to a great extent, so the first-principles self-consistent calculation of the electronic structure of defects is possible with the use of the LMTO TB method.

It is convenient to use the atomic-sphere approximation (ASA) in the framework of the LMTO scheme. In this approach, each atom is surrounded by a sphere with volume equal to that of the Wigner–Seitz cell, and it is assumed that all space can be filled with these spheres, the overlapping of spheres of different atoms being neglected. The latter means that, effectively, there are no interstitial regions. In practice, the errors in the determination of the electron energy in the framework of the ASA does not exceed 1% of the width of the corresponding band. However, this approximation is valid only in the case of close-packed structures (FCC, BCC and HCP). For the calculation of electronic structure in the case of open structures, such as the diamond structure, it is necessary to introduce so-called empty spheres in the interstitial sites of a crystalline lattice in addition to spheres containing ions. These spheres contain no ion cores, but have some electron charge, as the self-consistency is achieved. Thus, the application of empty spheres is the practical tool for the more correct consideration of electron density outside the atomic spheres [19]. For crystals with a diamond structure, the empty spheres are placed at the tetrahedral void sites, so a close-packed structure of the BCC type is formed. Whereas the ASA serves well for crystalline silicon [19], this is not necessarily so for the grain boundaries because of the distorted and more open structure than in a perfect crystal. Taking this fact into account, we have adjusted the positions and radii of empty spheres in the grain-boundary region so that the excess volume was taken into consideration and large sphere overlaps were avoided. Sphere radii at a grain boundary change in the range of $(0.999–1.06)R_{Si}$ only (where R_{Si} is the empty sphere radius in an ideal lattice) because of a small distortion on the investigated boundary, atomic sphere radii being constant. Therefore, the obtained structure is like the closely packed one and in this case the ASA could be quite accurate. A similar approximation (but without sphere radii adjustment) was used in [27] for amorphous silicon, which is characterized by distortions of the bond length ($\approx$3.1%) and deviations of the angles between the bonds ($\approx$17.7°) similar to the maximum ones in the structure of the investigated boundary. It has been shown that even this approach provides for the description of the electronic properties of amorphous silicon quite well. Also, this approximation (but without the self-consistent procedure) has been used for the study of the structure and energy of the $\Sigma 5\{1\,0\,0\}$ grain boundary in copper [28]. Hence we expect our approach to be correct enough for the calculation of the grain-boundary electronic structure.

In the framework of the LMTO TB ASA method, the basis functions are constructed from solutions of the Schrödinger equation inside the Wigner–Seitz spheres. The minimal basis set for a covalent crystal in this method contains s, p and d orbitals at the atomic sites and s and p orbitals at the interstitial sites. However, it was shown [29] that it is possible to use a smaller basis set to calculate one-electron energies and wavefunctions without a significant decrease in accuracy if higher partial waves were taken into account by a procedure equivalent to Löwdin partitioning or block perturbation theory [30]. This procedure allows one to reduce the size of the matrices that are diagonalized and

therefore decrease the computational time by an order of magnitude in comparison with the conventional LMTO method, which is extremely important for the calculation of the electronic structure of grain boundaries.

We now briefly describe the practical scheme that we used for the calculation of the grain-boundary electronic structure in silicon. A detailed description of the LMTO TB method is given in [18, 19]. The basis orbital in the TB representation, $\chi^{\alpha}_{RL}(r-R)$, centred at lattice site R and with the abbreviation $L=\{l, m\}$ for the angular momentum (l) and azimuthal (m) quantum numbers, is a superposition of the conventional LMTO, and is given by the one-centre expansion:

$$|\chi^{\alpha}_{RL}\rangle^{\infty} = |\Phi_{RL}\rangle + \sum_{R'L'} |\dot{\Phi}^{\alpha}_{R'L'}\rangle h^{\alpha}_{R'L'RL} \tag{1}$$

where $|\chi^{\alpha}_{RL}\rangle^{\infty}$ extends over all space, while $|\Phi_{RL}\rangle$ and $|\dot{\Phi}^{\alpha}_{R'L'}\rangle$ are non-zero only in their own atomic spheres. Here $\Phi_{RL}(r_R) = \Phi_{Rl}(r_R)Y_L(\hat{r}_R)$, where Φ_{Rl} is the regular solution of the radial Schrödinger equation in the sphere for the fixed but arbitrary energy $E_{\nu kl}$ chosen at the centre of interest; Y_L are the spherical harmonics; $r_R \equiv (r-R)$ and $r_R \equiv |r_R|$. The Φ_{RL} is normalized to unity in its sphere as

$$\langle\Phi_L|\Phi_L\rangle \equiv \int_{\Omega} \Phi^*_L(r)\Phi_L(r)\,\mathrm{d}r = \int_0^s |\Phi_l(r)|^2 r^2\,\mathrm{d}r = 1 \tag{2}$$

where s is the radius of an atomic sphere.

The $\dot{\Phi}^{\alpha}_{RL}$ is defined as a superposition of Φ_{RL} and its energy derivative function $\dot{\Phi}_{RL}$:

$$\dot{\Phi}^{\alpha}_{RL}(r_R) = \dot{\Phi}_{RL}(r_R) + \Phi_{RL}(r_R)o^{\alpha}_{Rl}. \tag{3}$$

The values of the potential parameter o^{α}_{Rl} (see appendix) were chosen to make the tight-binding muffin-tin orbital energy derivative vanish.

The matrix h^{α}_{LL} (here and in the following, in a matrix notation the subscript R is dropped) in (1) was determined so that the TB LMTO is continuous and differentiable on the sphere:

$$h^{\alpha}_{LL} = -P^{\alpha}_L(\dot{P}^{\alpha}_L)^{-1} + (\dot{P}^{\alpha}_L)^{-1/2}S^{\alpha}_{LL}(\dot{P}^{\alpha}_L)^{-1/2}. \tag{4}$$

The values P^{α}_L and $\dot{P}^{\alpha}_L$ are the potential parameters (diagonal matrices), which are related to the conventional ones as given in the appendix.

The screened structure matrix S^{α}_{LL} is determined through the Dyson equation:

$$S^{\alpha}_{LL} = S^0_{LL} + S^0_{LL}\alpha_L S^{\alpha}_{LL} \simeq \alpha_L^{-1}[(\alpha_L^{-1} - S^0_{LL})^{-1} - \alpha_L]\alpha_L^{-1} \tag{5}$$

where S^0_{LL} is the conventional canonical structure matrix [18, 31], which is Hermitian and independent of the scale of the structure; α_L is a diagonal matrix with elements usually independent of R, and $\alpha_L \equiv 0$ for $l \geqslant 2$. The set of 'screening numbers' is found by the trial-and-error method [19] in such a way that the localization of S^{α}_{LL} is the best: $\alpha_s = 0.348485$, $\alpha_p = 0.053030$, $\alpha_d = 0.010714$.

Now, to obtain a down-folded basis it is necessary only to go to energy-dependent screening coefficients $\beta(E)$. Using the subscript notation L for the lower partial waves and H for the higher partial waves (in the case of silicon H = p for the empty spheres and H = d for the atomic sphere), it is specified by [29] that

$$\beta_L \equiv \alpha_L \qquad \beta_H(E) = [P^0_H(E)]^{-1} \tag{6}$$

where $P^0_H(E)$ is a conventional potential function [18]. The transformation of the one-centre expansion (1) to the $\beta(E)$ representation from the original α is given by substituting the structure matrix S^{α}_{LL} by the structure matrix $S^{\beta(E)}_{LL}$ defined as

$$S_{LL}^{\beta(E)} = S_{LL}^{\alpha} + S_{LH}^{\alpha} F_{HH}^{\alpha}(E) S_{HL}^{\alpha}$$
$$S_{HL}^{\beta(E)} = P_H^{\alpha}(E) F_{HH}^{\alpha}(E) S_{HL}^{\alpha} \tag{7}$$

where $F_{HH}^{\alpha}(E)$ is the 'higher-block Green function' [29]:

$$F_{HH}^{\alpha}(E) = [P_H^{\alpha}(E) - S_{HH}^{\alpha}]^{-1}. \tag{8}$$

Equation (4) in $\beta(E)$ representation is

$$h_{LL}^{\beta(E)} = -P_L^{\alpha}(\dot{P}_L^{\alpha})^{-1} + (\dot{P}_L^{\alpha})^{-1/2} S_{LL}^{\beta(E)} (\dot{P}_L^{\alpha})^{-1/2} \tag{9}$$

and in this case the basis function is found to be

$$|\chi_L^{\beta(E)}\rangle = |\Phi_L\rangle + |\dot{\Phi}_L^{\alpha}\rangle h_{LL}^{\beta(E)} + |\Phi_H\rangle \frac{(-1)}{(\Gamma_H^{\beta})^{1/2}} S_{HL}^{\beta(E)} \frac{1}{(\dot{P}_L^{\alpha})^{1/2}}. \tag{10}$$

Here Γ_H^{β} is the potential parameter (see appendix). The energy dependence in expressions (6)–(10) may be omitted by fixing $E = E_{\nu H}$.

Hamiltonian and overlap matrices can be obtained from (10) using the condition $E = E_{\nu H}$ in the form:

$$O_{LL}^{\beta} = (I + h_{LL}^{\beta} o_L^{\alpha})(o_L^{\alpha} h_{LL}^{\beta} + I) + h_{LL}^{\beta} p_L h_{LL}^{\beta} + (\dot{P}_L^{\alpha})^{-1/2} S_{LH}^{\beta} (1/\Gamma_H^{\beta}) S_{HL}^{\beta} (\dot{P}_L^{\alpha})^{-1/2} \tag{11}$$

and

$$H_{LL}^{\beta} = h_{LL}^{\beta} + h_{LL}^{\beta} o_L^{\alpha} h_{LL}^{\beta} + (I + h_{LL}^{\beta} o_L^{\alpha}) E_{\nu L} (o_L^{\alpha} h_{LL}^{\beta} + I) + h_{LL}^{\beta} E_{\nu L} p_L h_{LL}^{\beta}$$
$$+ (\dot{P}_L^{\alpha})^{-1/2} S_{LH}^{\beta} (V_H^{\beta}/\Gamma_H^{\beta}) S_{HL}^{\beta} (\dot{P}_L^{\alpha})^{-1/2} \tag{12}$$

where I is the unit matrix, V_H^{β} and p_L are defined in the appendix. One should note that functions defined by (10) are not the LMTO, because

$$\frac{\partial}{\partial E} |\chi_L^{\beta}(E)\rangle^{\times} \Big|_{E_{\nu}} \neq 0. \tag{13}$$

However, the accuracy of the determination of one-electron energies of lower partial waves is of the same order as that in the LMTO TB method. The inaccuracy for the higher partial waves is slightly more; however, the error does not exceed $(E - E_{\nu})^2$. A detailed consideration of this problem is given in [29].

It is necessary to determine the charge density at each step of the self-consistent calculation in the framework of DFT. It is possible to calculate it with the use of the spherically symmetric part obtained from the partial-wave expansion in the Wigner–Seitz (WS) sphere. Such an approach is convenient because it provides for a sufficient accuracy and the full, non-spherically averaged charge density has so far been difficult to represent throughout the cell and is not needed during a self-consistent calculation. The ASA total energy normally deviates from the proper total energy only by hundredths of a rydberg [19].

The distribution of the charge density of the valence electrons in the atomic sphere R, i.e. $\rho_R(r)$, in this approach can be described as

$$\rho_R(r) = \frac{1}{4\pi} \sum_l \int_0^{E_F} 2N_{Rl}(E) \Phi_{Rl}^2(r, E)\, dE \tag{14}$$

where Φ_{Rl} is the solution of the radial Schrödinger equation for the energy E; and $2N_{Rl}(E)$ is the local partial density of states determined by

$$N_{Rl}(E) = \frac{\Omega}{(2\pi)^3} \sum_l \int_{WS} C_{Rl}^{kj} \delta(E - E_j(k))\, dk \tag{15}$$

where Ω is the volume of the unit cell; and $E_j(k)$ is the one-electron energy of state j at point k. The expressions for the coefficients C_{Rl}^{kj} are given in the appendix.

Table 1. The main characteristics of the electronic band structure of single-crystal silicon, obtained with the use of different exchange–correlation potentials.

Variant no.	Type of potential[a]		Band-gap width (eV)	Valence band width (eV)	Width of direct gap at Γ point, $\Gamma_{15} - \Gamma_{25}$ (eV)
	Atomic spheres	Empty spheres			
1	V_{PZ}	V_{PZ}	0.52	12.28	3.52
2	V_{BH}	V_{BH}	0.63	12.23	3.50
3	V_{PZ}	V_{SI}	0.74	12.21	3.54
4	V_{BH}	V_{SI}	1.14	12.03	3.52
Experimental data [38]			1.17	12.5 ± 0.6	3.4

[a] V_{PZ} Perdew–Zunger exchange–correlation potential.
V_{BH} Barth–Hedin exchange–correlation potential.
V_{SI} Slater exchange–correlation potential with coefficient $\alpha = 0.7$.

The determination of the exchange–correlation potential is a very important problem in the calculation of the electronic structure of semiconductors. The point is that, if one investigates a semiconductor electronic structure in the framework of DFT, then the well known problem of a dielectric gap appears. This problem consists of the underestimation of the band-gap width by about 40–60%, which arises because of the substitution of the non-local self-energy operator by the local exchange–correlation potential [32, 33]. The contemporary state of theory does not allow one to determine unambiguously the form of the local exchange–correlation potential most suitable for the calculation of the electronic properties of solids. The only way to choose the potential type is via comparison of the calculated results with the experimental data. A number of approximations for the exchange–correlation potential have been proposed, and each of them is correct only for a definite type of electron charge density distribution. The open structure of silicon is characterized by a strongly non-uniform distribution of charge density. It changes rapidly in the atomic spheres and becomes approximately uniform and small in the empty spheres. So, it is reasonable to use different types of exchange–correlation potential for the atomic spheres and empty spheres, and a uniform distribution of electron density with small values is well described by a Slater-type potential [34]. One should note that similar approaches have been used for the investigation of the electronic structure of intermetallic compounds [35] and semiconductors [36].

We have carried out test calculations of the electronic band structure of a perfect crystal of silicon (with lattice constant equal to 5.43 Å) using different forms of the local exchange–correlation potential for both the atomic spheres and empty spheres. We continued the iterative calculations until self-consistency with $\Delta E_{tot} \leqslant 5 \times 10^{-3}$ eV was reached (ΔE_{tot} is the total energy per unit cell). The integration was carried out by the method of tetrahedra [37] through the 50 k-points of the 1/48th irreducible part of the Brillouin zone. The results of the test calculations are given in table 1.

The levels of the one-electron energy are seen to be strongly sensitive to the form of the exchange–correlation potential. Consideration of the results obtained with the variants 1 and 2 of the exchange–correlation potentials (table 1) shows that the width of the direct energy gap at the point Γ is in good agreement with the experimental value, while the estimation of the band gap has significant discrepancies in comparison with the experimental data (the underestimation of the band-gap width is 55.6 and 46.2% for variants 1 and 2 of the exchange–correlation potential, respectively).

Table 2. One-electron energy of single-crystal silicon at the characteristic points of the Brillouin zone relative to the energy of the top of the valence band (Γ'_{25} point).

Point	Present work (eV)	Theory [41] (eV)	Experiment [38] (eV)
Γ_1	−12.03	−11.99	−12.5 ± 0.6
Γ_{15}	3.52	2.50	3.4
Γ'_2	3.77	3.21	4.2
X_{1v}	−7.93	−7.84	—
X_{4v}	−2.79	−2.88	−2.9 ± 0.2
X_{1c}	1.23	0.55	1.3
L'_2	−9.62	−9.64	−9.3 ± 0.4
L_{1v}	−6.93	−7.04	−6.7 ± 0.2
L_3	−1.03	−1.21	−1.2 ± 0.2
L_{1c}	1.77	1.41	2.1 ± 0.15
L'_1	3.85	3.26	4.15 ± 0.1
Band-gap width (eV)	1.14	0.41	1.17

The application of the Perdew–Zunger [39] or Barth–Hedin [40] exchange–correlation potentials for the atomic spheres along with the Slater potential [34] for the empty spheres (variants 3 and 4 in table 1, respectively) leads to a significant decrease in the error of the estimation of the band-gap width. In the case of variant 4 (table 1) the error amounts to 2.5%, which represents a good fit with the experimental data.

This effect is caused by the increase of the potential inside the empty spheres owing to the increase of the correlation part in the exchange–correlation potential, if the Perdew–Zunger or Barth–Hedin potential are substituted by the Slater one. As a result, the potential barrier between the atomic spheres and empty spheres increases and this effect causes localization of wavefunctions inside atomic spheres and both narrowing and lowering of electronic bands. The opposite effect in the empty spheres is negligible. As a result, the width of the valence band decreases, it displaces in the direction of low energies and thus the width of the band gap increases. The decrease in the valence band width is rather small, and all the obtained values correspond to the experimental estimations. It is necessary to note that the effect of the application of the Slater potential for the empty spheres in variant 3 of the potential set (table 1) is lower than in variant 4. Hence, the application of the combination of different exchange–correlation potentials for the atomic spheres and empty spheres provides for the increase of the accuracy of the band-structure determination for silicon owing to a more correct description of the electron density distribution in the unit cell.

The one-electron energies in silicon in several points of the Brillouin zone obtained with the application of the Barth–Hedin exchange–correlation potentials for the atomic spheres along with the Slater potential for the empty spheres are given in table 2. The energy of the state Γ'_{25} (the top of the valence band) is taken as the zeroth energy. The results of the presented work are seen to be in better agreement with the experimental data than that obtained in [41] with the use of an exchange–correlation potential of Gaspar–Kohn–Sham type [42]. The calculation of the cohesive energy per atom with the use of these exchange–correlation potentials has given us the value of 4.8 eV, which corresponds to ≈3.7% overestimation in comparison with the experimental data.

The self-consistent calculation of the grain-boundary electron structure was carried out up to the same level of self-consistency as for the test calculation with the Barth–

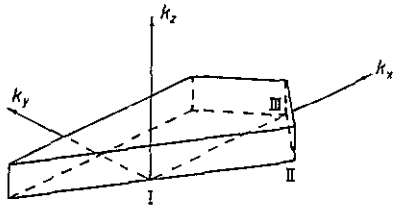

Figure 2. The 1/2 irreducible part of the Brillouin zone of the supercell used for calculation of the electronic structure of the Σ5 {2 1 0} boundary: I, (0, 0, 0); II, $2\pi/a(4/5, -1\sqrt{5}, 0)$; III, $2\pi/a(6/5, 0, 0)$.

Hedin exchange–correlation potentials for the atomic spheres and the Slater potential with $\alpha = 0.7$ for the empty spheres.

In the supercell method the periodicity normal to the boundary plane is imposed in addition to the two-dimensional periodicity in the boundary plane. The supercell used for the calculation of the grain-boundary electron structure had an inversion centre and contained two oppositely misoriented Σ5 {2 1 0} grain boundaries spaced by 16 atomic planes. Thus, a fully periodic structure was obtained. The Brillouin zone of the supercell obtained has the shape of a hexagonal prism. The irreducible part of this Brillouin zone is shown in figure 2. Choosing the thickness of the supercell in the present work we took into account the value of the radius of vanishing of the basis functions of the LMTO TB method. For silicon, the LMTO TB basis orbital extends to third-nearest neighbours [19], and we choose the thickness of the supercell so that the grain-boundary cores in it were separated by a region of the silicon lattice with thickness exceeding two radii of the third coordination sphere; thereby one ensures the absence of a region of mutual influence of grain boundaries in the supercell.

The integration was carried out through the 29 k-points of the 1/2 irreducible part of the Brillouin zone (figure 2) in the plane $k_z = 0$ by the triangle method with linear interpolation, because the preliminary test calculation had shown a negligibly small dispersion along the k_z direction (about 10^{-3} Ryd). The test calculation with a varying number of k-points has shown that the integration error does not exceed 10^{-3} Ryd. Therefore, we believe that the calculation of the main electronic properties of a grain boundary was carried out accurately enough.

3. Results

The local density of states is important for the understanding of numerous properties. In particular, being a local characteristic for an electron structure it is more sensitive to different local distortions of the regular crystal lattice order and enables us to carry out a more detailed description of localized and resonant defect states in comparison with energy band structure. In figure 3 the data for the local density of states at atoms 0–3, 5 and 8 are presented. Though the rigid-body translation disturbs the symmetry of the boundary plane, the atoms in pairs 1 and 1^-, 2 and 2^-, etc (figure 1) became inequivalent, but the local density of states on them differs insignificantly. In figure 3 the data for the atoms on the side of the boundary characterized by the strongest distortions of the atomic coordination are presented.

The following features of the local density of states in the valence band were observed:

(i) A splitting of the s peak occurs into peaks 1 and 2 (figure 3) with a shift of peak 2 in the direction of increasing energy and peak 1 in the opposite direction. The splitting of the s peak is the strongest on atom 0. This effect is weaker on the neighbouring atoms and obviously exists mainly due to the interaction with atom 0.

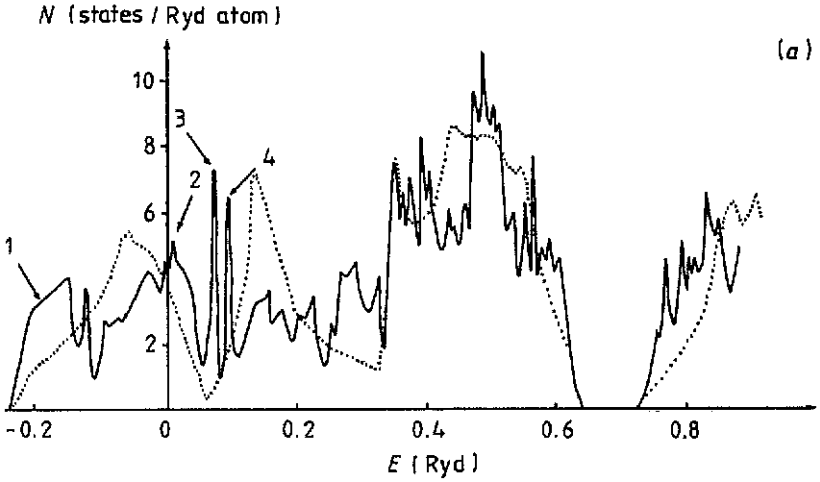
N (states / Ryd atom)
(a)
10
8
6
2
1
2
3
4
-0.2
0
0.2
0.4
0.6
0.8
E (Ryd)

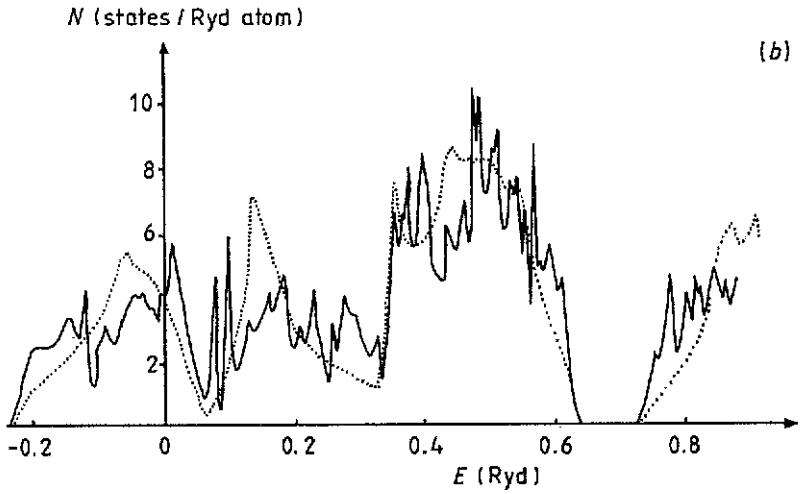
N (states / Ryd atom)
(b)
10
8
6
2
-0.2
0
0.2
0.4
0.6
0.8
E (Ryd)

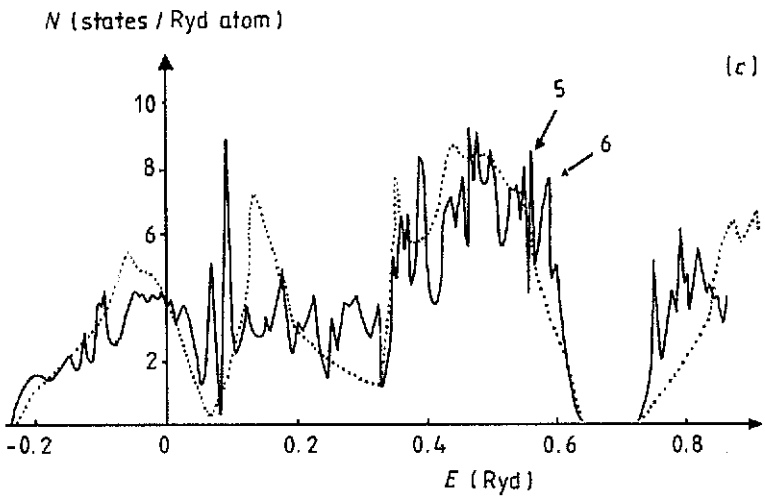
N (states / Ryd atom)
(c)
10
8
6
2
5
6
-0.2
0
0.2
0.4
0.6
0.8
E (Ryd)

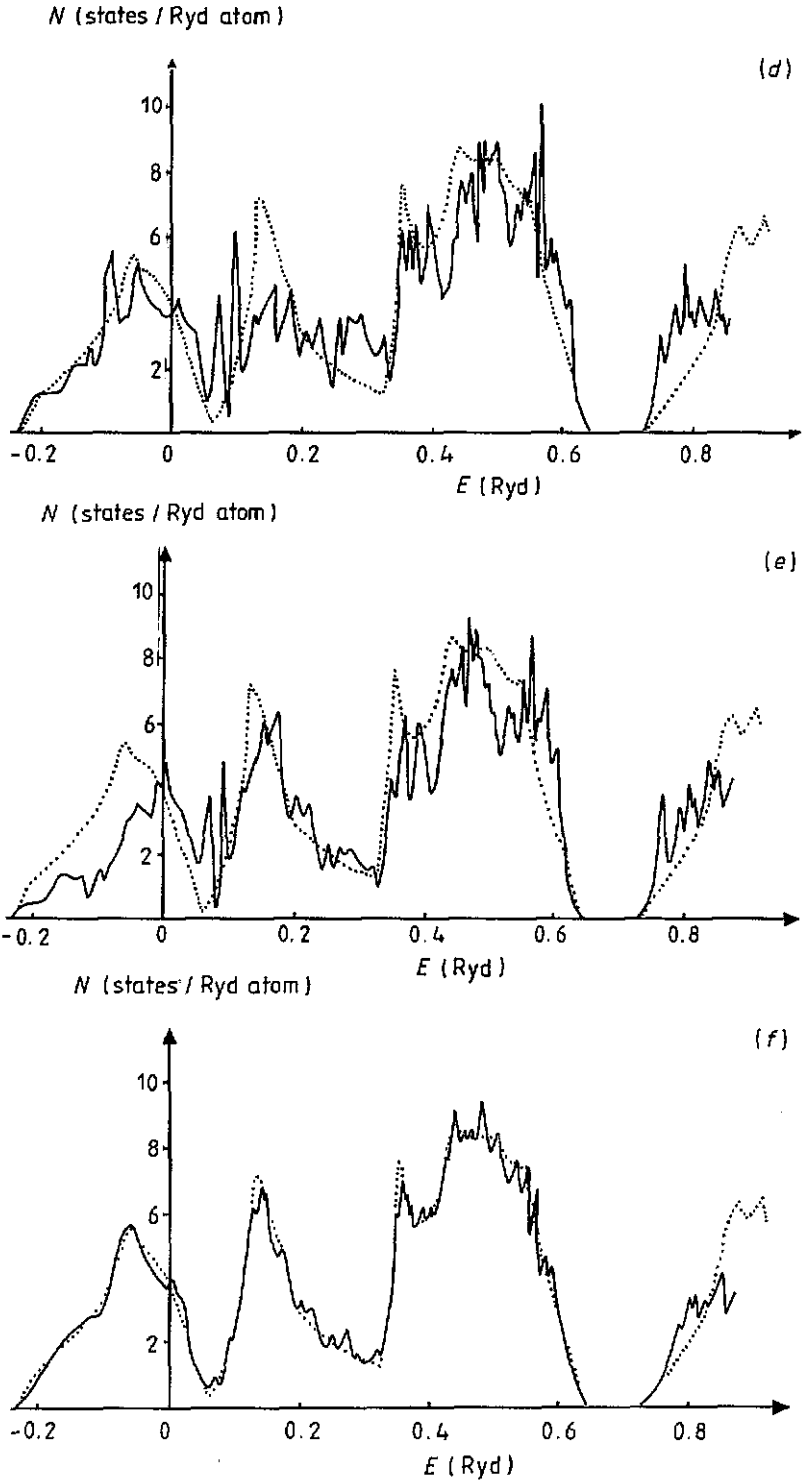

Figure 3. Local densities of states N on atoms 0 (*a*), 1 (*b*), 2 (*c*), 3 (*d*), 5 (*e*) and 8 (*f*), as numbered in figure 1. Dotted curves show the density of states in the perfect crystal. Numbered state peaks are shown by arrows.

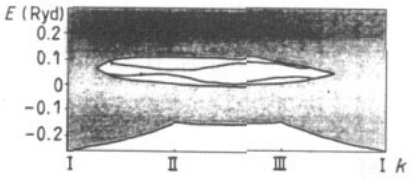

Figure 4. Interfacial electronic structure near the pseudo-gap of a single crystal. The projections of the bulk bands are shaded.

(ii) Sharp and high s-type peaks (peaks 3 and 4, figure 3) appear in the region of the minimum of the state density related to a pseudo-gap in a single crystal (figure 4). In figure 4 the fragment of the band structure of the examined supercell in this energy region is shown. We can see two defect states with energy equal to that of peaks 3 and 4. The state of peak 3 is situated closer to the edge of the pseudo-gap (to the electron state of a single crystal) and has a lower energy dispersion.

(iii) A dissipation of the s–p hybridized peak is seen along with a significant reduction of the maximum density of states. In this energy region low s–p peaks were formed up to the low-energy edge of the p peak of a single crystal. According to [27], such a character of the distribution of the density of states is also typical for amorphous silicon.

(iv) A number of small sharp peaks are observed in the valence band, including peaks with p symmetry near the top of the band (peaks 5 and 6, figure 3).

All effects observed in the local density of states are decreasing, moving away from the grain boundary. So, atom number 8 has almost the same density of states as a single crystal with a slight difference. It seems to be related to the different number of points used for integration through the Brillouin zone in the cases of the grain boundary and single crystal.

We analysed the dependence of the state density with fixed energy values versus the distance from the grain boundary. Figure 5 shows that the states of peaks 3 and 4 are localized defect states. Their state density rapidly decreases with distance from the atoms on which they are formed. The state of peak number 3 is localized on atom number 0. This atom is characterized by the highest angle deviation of the bonds from the single-crystal value. Peak number 4 is associated with atoms number 2 and 2^-, which have the strongest distortion of the bond length with the neighbours in comparison with the ideal bond length.

The heights of peaks 1, 2, 5 and 6 decrease slightly oscillating with distance from the grain boundary. Such behaviour is characteristic of resonance states. The spatial decrease of the heights of peaks 1, 2, 5 and 6 agrees with the positions of the corresponding states in the energy region of the filled part of the single-crystal valence band. The state of peak 5 is localized on atoms 3 and 3^-, and peak 6 has highest intensity at atoms 2 and 2^-.

The charge distribution at the Si atoms is shown in figure 6. The variation in this quantity should be a good measure of the charge fluctuation in a grain-boundary structure from one atom to another because the atomic sphere radii do not change [27]. At the same time, such a comparison of the charges in the empty spheres does not have any meaning because their radii are different. It is seen that the deviation of the charge value at the atoms of the grain boundary from that of a single crystal is about $\pm 0.1e$, where e is the electron charge. A positive charge exists on the Si atoms in a single crystal owing to the transference of a part of the electron charge from atoms to the states of empty spheres. An excess negative value was found on atoms 0, 1^- and 1 with a value of the bond tension of 2.1% and a strong distortion of the angles between the bonds. In contrast, at the atoms 2, 2^-, 5 and 5^- with a strong tension of bonds the lack of electron

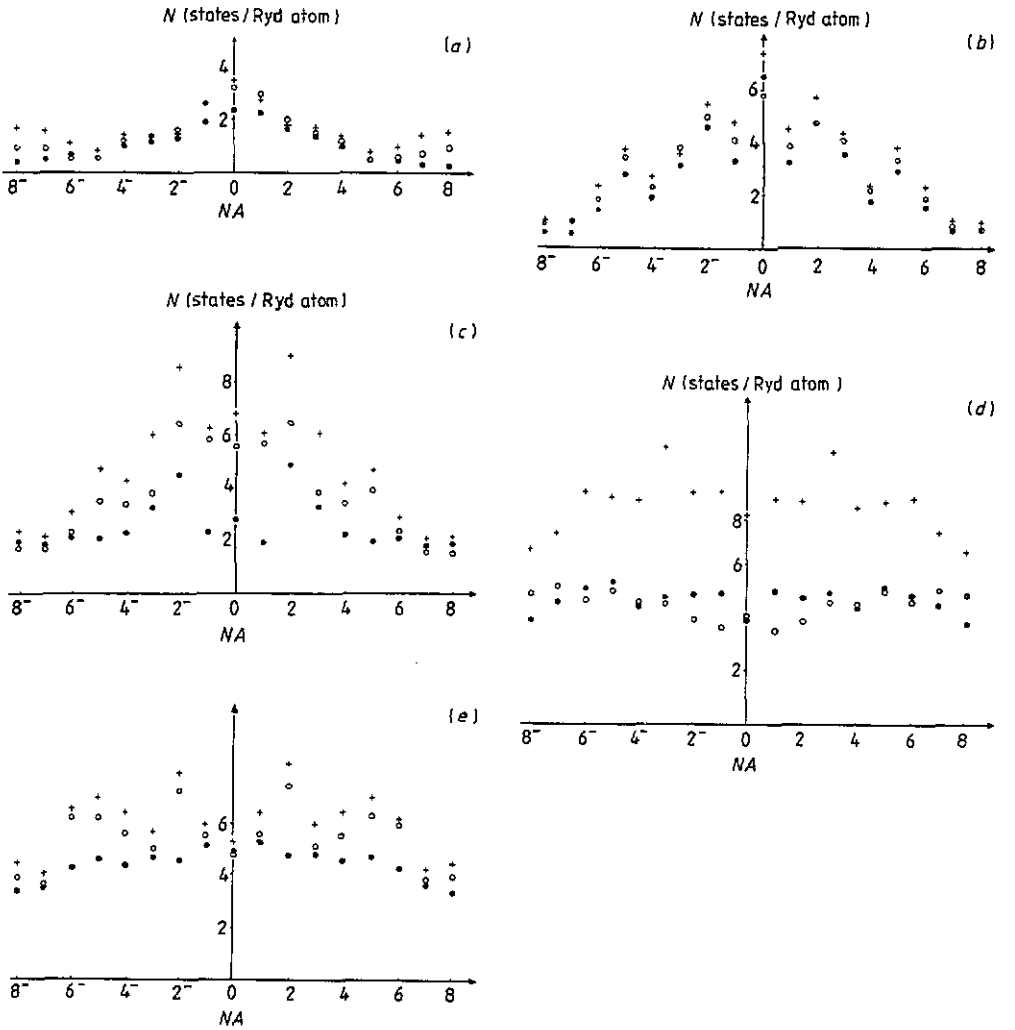

Figure 5. The dependence of the local density of states N with fixed energy values E on the positions of the atoms in the grain-boundary structure: (*a*) peak 1, (●) $E = -0.225$ Ryd, (○) $E = -0.20$ Ryd, (+) $E = -0.175$ Ryd; (*b*) peak 3, (○) $E = 0.07$ Ryd, (+) $E = 0.0725$ Ryd, (●) $E = 0.075$ Ryd; (*c*) peak 4, (○) $E = 0.09$ Ryd, (+) $E = 0.095$ Ryd, (●) $E = 0.10$ Ryd; (*d*) peak 5, (○) $E = 0.555$ Ryd, (+) $E = 0.560$ Ryd, (●) $E = 0.565$ Ryd; (*e*) peak 6, (○) $E = 0.585$ Ryd, (+) $E = 0.590$ Ryd, (●) $E = 0.595$ Ryd. *NA* = number of atom (figure 1).

charge is observed. The maximum deviation of the charge from the single-crystal value is observed at atom 5, which has tension of the bond with atom 2 of 3.2%. The dependence of charges of the atoms on distance from the boundary is slightly asymmetric. It is related to the asymmetry of the atomic structure caused by the rigid-body translation in a boundary plane.

The charge values almost converge to the perfect crystal value at the eighth plane. On the basis of the dependence of local state densities and charge value on distance from the grain boundary, we can say that the region of the electronic distortions associated with this boundary is about 12–14 atomic planes (6–7 atomic planes on each side of the

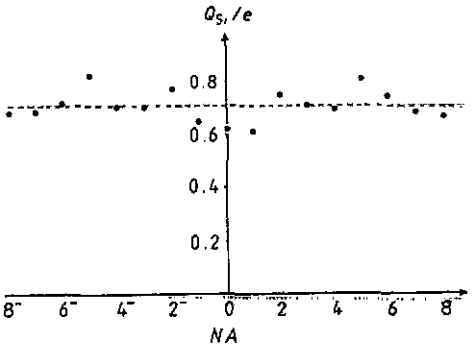

Figure 6. The charges of the atomic spheres Q_{Si} in the grain-boundary structure in terms of electron charge e. The broken line shows the charge of Si atomic spheres in a single crystal. NA = number of atom (figure 1).

Table 3. The ratio of occupancy values of the p states and s states ($f_{p/s}$) on atoms at the $\Sigma 5$ {2 1 0} grain boundary.[a]

Numbers of atoms	0	1	2	3	4	5	6	7	8
$f_{p/s}$	1.57	1.63	1.50	1.55	1.62	1.51	1.58	1.60	1.63

[a] $f_{p/s}$ in a single crystal is equal to 1.64.

grain junction plane), or about 1 nm. This value is more than the geometrical boundary thickness, but much less than the electrical thickness of electrically active boundaries [43].

The formation of additional defect s states at the boundary leads to a change of hybridization state of several atoms. The ratio of the occupancy of states of p symmetry to the occupancy of s-symmetry states ($f_{p/s}$) on atoms 0–8 is given in table 3.

It is seen that both the excess charge on atom 0 and the lack of charge on atoms 2 and 5 were caused mainly due to the changes in the relative occupancy of the s-symmetry orbitals. Uniform changes of occupancy of the p and s states take place only on atom 1. A similar behaviour of the $f_{p/s}$ was observed in the $\Sigma 3$ {2 1 1} grain boundary in silicon [2]. This behaviour confirms the assumption that the bonding of atoms in the region of a highly distorted structure is provided by the enhanced occupancy of the spherically symmetric s orbitals [44]. The same phenomenon was found in the electronic structure of grain boundaries in Ni_3Si and Ni_3Al [44].

This effect becomes especially important for the boundaries, which can have two types of structure with approximately the same energy values if the first type has a strongly distorted tetrahedral packing and the second one has a local configuration of black lead type around some atoms. For example, such a situation can be observed in silicon in the $\Sigma 11$ {3 1 1} boundary with and without a reconstruction [45] and in the $\Sigma 33$ {8 1 1} boundary [46].

Our calculations have shown that the excess energy of the $\Sigma 5$ {2 1 0} boundary, estimated in the framework of the density-functional theory based on data for the density of electron states, is 460 ± 40 erg cm^{-2}. The calculation of its energy by the bond orbital model gave the value of 1200 erg cm^{-2}. Such a great difference between the results obtained with the use of the self-consistent LMTO TB calculation and empirical methods is related to the changes in the electron structure due to changes of atomic coordination, which were not taken into account in the latter case. It points out the great significance of electron system relaxation.

4. Discussion

Our results for Σ5 {2 1 0} together with the data for Σ5 {3 1 0} of Paxton *et al* [2] and Kohyama *et al* [9] have not revealed any proper boundary states in the band gap. Summarizing these results, we can expect a similar behaviour of all symmetric tilt ⟨1 0 0⟩ boundaries in silicon. This assumption is based on the fact that structure units of Σ5 (and a single crystal) form the structure of all boundaries belonging to this class [20]. It can cause the electrical passivity of these boundaries. It is true only for equilibrium boundaries without any additional defects. The electron-beam-induced current (EBIC) and transmission electron microscope (TEM) studies of the ⟨1 0 0⟩ tilt grain boundaries with Σ5, 13, 25 [47, 48] have shown that the electrical activity of these boundaries was caused by extrinsic dislocations or precipitates.

The problem of the existence of a correlation between the character of the local distortions of the atomic structure and local characteristics of the electronic structure has been disputable up to now [49, 50]. Our results have revealed the absence of an unambiguous simple relationship of such a character. In particular, different types of atomic arrangement can cause similar effects in an electronic structure. For example, atom 0 (figure 1) has a strong distortion of the angles between the bonds, but small changes of the bond length. Atom 2 has a strong tension of the bond with atom 2^-, and a low deviation of the angles between bonds. Despite this, the local electronic structures are similar in both these positions, so the high sharp peaks (3 and 4, figure 3) of s-like states are localized at atoms 0 and 2. At the same time, a relatively strong tension of the bond on atom 5 (of 3.2%) causes another effect, i.e. the shift of the s peak in the direction of high energies.

It should be noted that, analysing the local electronic structure at an atom in the boundary, we must take into account the complex picture of the atomic structure. The different types of distortions in the grain-boundary structure interact with each other and so we cannot separate the influence of an angle distortion, bond tension, etc, on the electronic structure. It is not an essential feature of grain boundaries, because the same conclusion was drawn for the electronic states of amorphous semiconductors [27]. This ambiguity of the relationships between the atomic and electronic structures concerns the quantitative redistribution of the density of states inside a valence band; therefore, the aforementioned conclusions drawn on the principal character of the electronic structure of ⟨1 0 0⟩ symmetric tilt boundaries remain true.

Appendix

All the potential parameters used in this work can be determined on the basis of the four conventional potential parameters:

$$p_l \equiv \langle \dot{\Phi}_{vl}^2 \rangle = -\ddot{\Phi}_{vl}/3\Phi_{vl}$$

$$\gamma_l \equiv \frac{(S/\omega)^{2l+1}}{2(2l+1)} \frac{D_{\dot{v}l} - l}{D_{\dot{v}l} + l + 1}$$

$$C_l \equiv E_{vl} - \frac{\Phi_{vl}}{\Phi_{\dot{v}l}} \frac{l + 1 + D_{vl}}{l + 1 + D_{\dot{v}l}}$$

$$\Delta_l^{1/2} \equiv \frac{(S/\omega)^{2l+1}}{2(2l+1)} \left(\frac{\omega}{2}\right)^{1/2} \Phi_{vl} \frac{D_{\dot{v}l} - D_{vl}}{l + 1 + D_{\dot{v}l}}$$

where

$$D_{\nu l} = S\,\Phi'_{\nu l}/\Phi_{\nu l} \qquad D_{\dot\nu l} = S\,\dot\Phi'_{\nu l}/\Phi_{\nu l}$$

ω is the mean radius of the Wigner–Seitz cell, S is the radius of the atomic sphere, and

$$\Phi_{\nu l} = \Phi_l(E_\nu, S)$$

$$\dot\Phi_{\nu l} = \frac{\partial}{\partial E}\Phi_l(E,S)\bigg|_{E=E_\nu}$$

$$\Phi'_{\nu l} = \frac{\partial}{\partial r}\Phi(E_\nu, r)\bigg|_{r=S}.$$

The screened potential parameters can be determined as

$$[P_l^\alpha(E)]^{-1} = \Delta_l/(E - C_l) + \gamma_l - \alpha_l \qquad [\dot P_l^\alpha(E)]^{-1} = (E - V_l^\alpha)/(\Gamma_l^\alpha)^{1/2}$$

where

$$V_l^\alpha \equiv C_l - \Delta_l/(\gamma_l - \alpha_l) \qquad \Gamma_l^\alpha \equiv \Delta_l/(\gamma_l - \alpha_l)^2$$

$$V_H^\beta \equiv C_H - \Delta_H/[\gamma_H - (P_H^0)^{-1}] \qquad \Gamma_H^\beta \equiv \Delta_H/[\gamma_H - (P_H^0)^{-1}]^2$$

$$o_l^\alpha = 1/(V_l^\alpha - E_{\nu l}).$$

Coefficients C_{Rl}^{kj} in equation (15) are determined by

$$C_{Rl}^{kj} = \frac{1}{N_q}\sum(|W_{ql}^{kj}|^2 + \langle\dot\Phi_{Rl}^2\rangle|B_{ql}^{kj}|^2).$$

Here N_q is the number of atoms in the unit cell of the same type as atom $\boldsymbol{R}$; $\boldsymbol{q}$ are the coordinate vectors of such atoms.

The coefficients W_{ql}^{kj} and B_{ql}^{kj} are involved in the one-centre expansion of the wavefunction:

$$\Psi_R^{kj}(r) = \sum_L [W_{ql}^{kj}\Phi_{RL}(r) + B_{RL}^{kj}\dot\Phi_{RL}(r)]$$

and can be obtained from

$$W_{RL}^{kj} = b_{RL}^{kj} + o_{Rl}^\alpha \sum_{R'L'} S_{RLR'L'}^\alpha b_{R'L'}^{kj}$$

$$B_{RL}^{kj} = \sum_{R'L'} S_{RLR'L'}^\alpha b_{R'L'}^{kj}$$

where $b_{R'L'}^{kj}$ are the eigenvectors of the valence state j of the electron.

References

[1] Paxton A T and Sutton A P 1988 *J. Phys. C: Solid State Phys.* **21** L481
[2] Paxton A T and Sutton A P 1989 *Acta Metall.* **37** 1693
[3] Mauger A, Bourgoin J C, Allan G, Lannoo M, Bourret A and Billard L 1987 *Phys. Rev.* B **35** 1267
[4] Artemyev A V, Bogaturiantc A A, Vekilov Yu H, Nikolaeva A V and Fionova L K 1989 *Fiz. Tverd. Tela* **31** (9) 101
[5] Artemyev A V, Polyak L E and Fionova L K 1990 *Coll. Phys. Suppl.* **51** C1 71
[6] Chadi D J 1978 *Phys. Rev. Lett.* **41** 1062
[7] Chadi D J 1984 *Phys. Rev.* B **29** 785

[8] Kohyama M, Yamamoto R, Watanabe Y, Ebata Y and Kinoshita M 1988 *J. Phys. C: Solid State Phys.* **21** L695
[9] Kohyama M, Yamamoto R, Ebata Y and Kinoshita M 1988 *J. Phys. C: Solid State Phys.* **21** 3205
[10] Thompson R E and Chadi D J 1984 *Phys. Rev.* B **29** 889
[11] Korringa J 1947 *Physica* **13** 392
Kohn W and Rostoker N 1954 *Phys. Rev.* **94** 1111
[12] Slater J C 1937 *Phys. Rev.* **51** 846
[13] Lambrecht W R L and Anderson O K 1986 *Surf. Sci.* **178** 256
[14] Fujiwara T 1986 *J. Phys. F: Met. Phys.* **16** 869
[15] Skriver H L and Rosengaard N M 1991 *Phys. Rev.* B **43** 9538
[16] Holland B, Greenside H S and Schluter M 1984 *Phys. Status Solidi* b **126** 511
[17] DiVincenzo D P, Alerhand O L, Schluter M and Wilkins J W 1986 *Phys. Rev. Lett.* **56** 1925
[18] Andersen O K, Jepsen O and Glotzel D 1985 *Highlights of Condensed Matter Theory* ed F Bassani, F Fumi and M P Tosi (New York: North-Holland) pp 59–176
[19] Andersen O K, Pawlowska Z and Jepsen O 1986 *Phys. Rev.* B **34** 5253
[20] Kohyama M 1987 *Phys. Status Solidi* b **141** 71
[21] Kohyama M, Yamamoto R and Doyama M 1986 *Phys. Status Solidi* b **136** 31
[22] Kohyama M, Yamamoto R and Doyama M 1986 *Phys. Status Solidi* b **137** 11
[23] Harrison W A 1980 *Electronic Structure and the Properties of Solids* (San Francisco: Freeman)
[24] Kohyama M, Yamamoto R, Ebata Y and Kinoshita M 1988 *Trans. ISIJ* **28** 836
[25] Weins M J 1972 *Surf. Sci.* **31** 138
[26] Hohenberg P and Kohn W 1964 *Phys. Rev.* B **136** 864
[27] Bose S K, Winer K and Anderson O K 1988 *Phys. Rev.* B **37** 6262
[28] Yoonsik O H and Vitek V 1988 *Mater. Res. Soc. Symp. Proc.* **122** 97
[29] Lambrecht W R L and Andersen O K 1986 *Phys. Rev.* B **34** 2439
[30] Löwdin P O 1951 *J. Chem. Phys.* **19** 1396
[31] Andersen O K, Jepsen O and Sob M 1987 *Proc. Int. School on Electronic Band Structure Calculations and Their Applications (Lecture Notes in Physics 283)* ed M Junssonff (Berlin: Springer)
[32] Sham L J and Kohn W 1966 *Phys. Rev.* **145** 561
[33] Mazin I I, Maksimov E G, Savrasov S Yu and Uspenskii Yu A 1987 *Fiz. Tverd. Tela* **29** (9) 2629
[34] Slater J C 1951 *Phys. Rev.* **81** 385
[35] Nemoshkalenko V A and Antonov V N 1982 *Izv. Vuzov. Fiz.* **24** (12) 79
[36] Ali Dahr A I and Lee P M 1988 *Phys. Scr.* **38** 441
[37] Macdonald A H, Vosko S H and Coleridge P T 1979 *J. Phys. C: Solid State Phys.* **12** 2991
[38] Hybert M S and Louie S G 1986 *Phys. Rev.* B **34** 5390
[39] Perdew J P and Zunger A 1981 *Phys. Rev.* B **23** 5048
[40] Barth V and Hedin L 1972 *J. Phys. C: Solid State Phys.* **5** 1629
[41] Shen Y T, Bylander D M and Kleinman L 1987 *Phys. Rev.* B **36** 3465
[42] Gaspar R 1954 *Acta Phys. Acad. Sci. Hung.* **3** 263
Kohn W and Sham L J 1965 *Phys. Rev.* A **140** 1133
[43] Matare H F 1984 *J. Appl. Phys.* **56** 2605
[44] Eberhart M E and Vvedensky D D 1987 *Phys. Rev. Lett.* **58** 61
[45] Moller H J 1982 *J. Physique Coll.* **43** C1 33
[46] Kohyama M, Yamamoto R and Doyama M 1986 *Phys. Status Solidi* b **138** 387
[47] Maurice J L and Colliex C 1989 *Polycrystalline Semiconductors (Springer Proc. Physics 35)* (Berlin: Springer) p 83
[48] Ihal A and Nouet G 1989 *Polycrystalline Semiconductors (Springer Proc. Physics 35)* (Berlin: Springer) p 77
[49] Weaire D and Thorpe M F 1971 *Phys. Rev.* B **4** 2508
[50] Singh J 1981 *Phys. Rev.* B **23** 4156